

Experimental Platform for Investigation of Low-Frequency Magnetic Field Effects on Cells

Hoang Vu Viet¹, Lubomír Kremnický² , Martin Bereta³ , Michal Teplan^{1*} 

¹*Institute of Measurement Science, Slovak Academy of Sciences, Bratislava, Slovakia*

²*Institute of Chemistry, Slovak Academy of Sciences, Bratislava, Slovakia*

³*Faculty of Health Sciences, Catholic University in Ruzomberok, Slovakia*

Abstract: This study presents a novel experimental platform designed to systematically investigate the effects of low-frequency (LF) magnetic fields (MFs) on biological systems. By overcoming key methodological challenges, including variability in environmental conditions and poor reproducibility, this platform sets a new standard for experimental reliability. It integrates precise temperature regulation, high MF homogeneity, and a modular structure, that ensures adaptability to diverse experimental setups. The platform was validated using *Saccharomyces cerevisiae* CCY 21-4-99 as a model organism, cultivated under controlled conditions with and without MF exposure. The minimal growth variations observed between chambers confirm the ability of the platform to maintain reproducible conditions and support statistically robust experimental designs. The platform can be applied to diverse biological systems and can be technically adapted to different experimental requirements, including different electromagnetic field sources. It provides a highly controlled environment for investigating the cellular and subcellular effects of LF MF, creating a solid foundation for future research into its biological mechanisms and potential applications.

Keywords: low-frequency magnetic fields, biological effects, experimental platform, *Saccharomyces cerevisiae*, environmental control, reproducibility

1. INTRODUCTION

Low-frequency (LF) magnetic fields (MFs), typically ranging from Hz to kHz, are ubiquitous in modern environments due to sources such as power lines, household appliances, and industrial equipment. Therefore, their potential biological effects are a topic of considerable research interest, especially with regard to their influence on cellular processes and long-term health consequences. While LF MFs are known to interact with biological tissues and potentially alter cellular functions, the causal relationships and underlying mechanisms remain controversial.

Biological responses to LF MFs have been reported across various domains, ranging from basic cellular functions to potential clinical applications. Several studies suggest that MFs can modulate cell behavior through interactions with ion channels, membranes, and the cytoskeleton, and influence processes such as gene expression, protein synthesis, and cellular signaling pathways [1]. Other studies have reported changes in cell proliferation [2]-[5], gene expression [6], and reactive oxygen species production [7].

Potential beneficial applications of MF exposure have been demonstrated in regenerative medicine [8], wound healing [9], and even tumor inhibition [10]. In addition, LF MFs have

been investigated for their role in non-invasive cancer therapies [11], cardiovascular treatments [12], and neuroprotective applications [13]. Conversely, epidemiological studies have shown an association between LF MF exposure and an increased risk of childhood leukemia [14], and neurodegenerative diseases [15], [16]. While mixed effects were observed for the immune system, negative effects were observed for the reproductive and cardiovascular systems [17]. The coexistence of beneficial and harmful effects underlines the need for systematic and well-controlled research. In addition to biomedical effects, the potential of LF MFs to improve microbial and plant biotechnological processes has also been explored, which would contribute to advances in food production, medicine, and environmental sustainability [18], [19].

Investigations at the molecular, subcellular, and cellular levels, as well as *in vivo* and epidemiological studies, have produced inconsistent results. Several review papers have attempted to identify the reasons for this lack of generally accepted conclusions. For example, Bodewein et al. [20] systematically analyzed the biological effects of electromagnetic fields in the intermediate frequency range (300 Hz to 1 MHz) and found that methodological limitations often

reduced the credibility of the reported results. While some results appear to be isolated, the comparison between other reports is contradictory and inconclusive [21], often due to variability in experimental setups, conditions, and biological models. The 2020 ICNIRP statement highlights the significant gaps in understanding the mechanisms of LF MF exposure and emphasizes the need for more robust experimental approaches [22]. This highlights the urgent need for a systematic, well-controlled, and reproducible approach to study the interactions of LF MF with biological systems, which has led several authors to propose improvements to various components of the experimental setups to improve precision and reproducibility [23], [24].

Since many open questions remain unanswered with existing tools, we have developed novel approaches in our previous studies to investigate the effects of electromagnetic fields on living systems. We have shown that LF MF affects biological autoluminescence (BAL), suggesting a potential link between electromagnetic exposure and cellular metabolic processes [25]. Although our measurement system allowed the monitoring of BAL, it was not able to follow the cell culture growth curves, which are crucial for the interpretation of biological responses. To address this, we introduced impedance spectroscopy for real-time cell concentration monitoring [26]. To assess cell cultures in liquid media using microscopic imaging, we developed an automated pipeline for decolorization and object segmentation [27]. Furthermore, we investigated the effects of pulsed electric fields on *Saccharomyces cerevisiae* and showed that BAL provides real-time insights into membrane permeabilization dynamics [28].

One of the main obstacles in this research field is the lack of rigorous control of experimental conditions. Factors such as temperature fluctuations within incubator spaces, background MFs from electronic devices, and variations in the Earth's magnetic field can obscure or confound the true effects of LF MF exposure. These uncontrolled variables contribute to the difficulty in reproducing results and hinder the development of universally accepted conclusions.

A variety of experimental setups are used in the literature, each with their own advantages and limitations. However, most of the MF bioeffect studies we reviewed – particularly those focusing on 50/60 Hz exposures (e.g., [2]-[4], [7], [11], [29]-[31]) – have not addressed temperature control in sufficient detail, raising concerns about the reliability of the reported thermal conditions. To overcome these challenges, there is a growing need for standardized methods and improved experimental systems that allow precise control of environmental and exposure parameters. In the present work, we place strong emphasis on precise temperature management and control to ensure the validity of the experimental conditions.

Based on our practical experience, we have developed and tested a simple experimental platform that ensures rigorous assessment and reproducibility of the effects of the LF MF while integrating standardized biological evaluation methods. In this study, we present the development and validation of the platform, addressing methodological limitations to improve research reliability. We describe the design, implementation, and evaluation of the platform and show that it is capable of supporting high-quality studies of the LF MF effects on biological processes.

2. MATERIALS AND METHODS

The workflow scheme

The workflow scheme (Fig. 1) outlines the design of a paired experiment suitable for the investigation of the effects of LF MF on microbial cultures. The workflow starts with a yeast strain from The Culture Collection of Yeasts (CCY) (Institute of Chemistry, Slovak Academy of Sciences, Slovakia) maintained on a solid medium in a Petri dish and used as inoculum for pre-cultivation.

After completing the pre-cultivation step, the yeast culture is diluted accordingly, distributed in vials, and placed in the cultivation chambers. The chambers are equipped with temperature regulation and temperature monitoring systems to ensure equal environmental conditions in both chambers. The integrated magnetic system enables the application of LF MF via two channels, both of which can be set to exposure or control mode. After cultivation, cell concentration measurements are performed, followed by subsequent data analysis with data control and filtration. Finally, selected data is subjected to statistical analysis.

Chemicals

YPD medium: 10 g yeast extract, 20 g peptone, 20 g glucose (M&B test a.s., Slovakia). YPD agar medium: 10 g yeast Extract (Biolife Italiana S.r.l., Italy), 20 g peptone (Peptone from meat, bacteriological, Sigma-Aldrich, Germany), 20 g D-glucose (Slavus s.r.o., Slovakia), agar 20 g (Agar Bios Special LL (Agar bacteriological), Biolife Italiana S.r.l., Italy) in 1 l medium. Trypan blue solution (Sigma-Aldrich, Germany).

Microbial strain and culture conditions

The *Saccharomyces cerevisiae* strain CCY 21-4-99 was cultivated in YPD medium at 35 °C and stored long-term on YPD agar in a Petri dish. Prior to the experiments, a full inoculation loop of the culture was transferred from the Petri dish to 50 ml of liquid YPD medium in a 100 ml Erlenmeyer flask. The flask was shaken to ensure homogeneity and then incubated statically at 35 °C. After 24 hours, the culture was rapidly cooled on ice, stored at 7 °C, and used as a pre-culture for further experiments within 4 to 10 days. The viability of the pre-culture was determined using a Bürker counting chamber after staining the cells with Trypan blue, with the percentage of viable cells ranging from 98.3 % to 99 %. Microbiological purity was assessed at each step of the experiment to ensure that no bacterial or fungal contamination was present visually and/or microscopically. In the rare cases where contamination occurred, the results were not taken into consideration. All experimental vials used for yeast cultivation were designed with flat bottoms to ensure an even distribution of growing cells. The cell cultures were immediately placed in an ice bath upon removal from the incubator to halt yeast cell growth prior to measurement. The biomass concentration was determined using a Bürker counting chamber or by turbidity measurement. The relationship between turbidity and cell concentration was established at 4.4×10^7 cells/ml, corresponding to 400 NTU, based on microscopic cell counting.

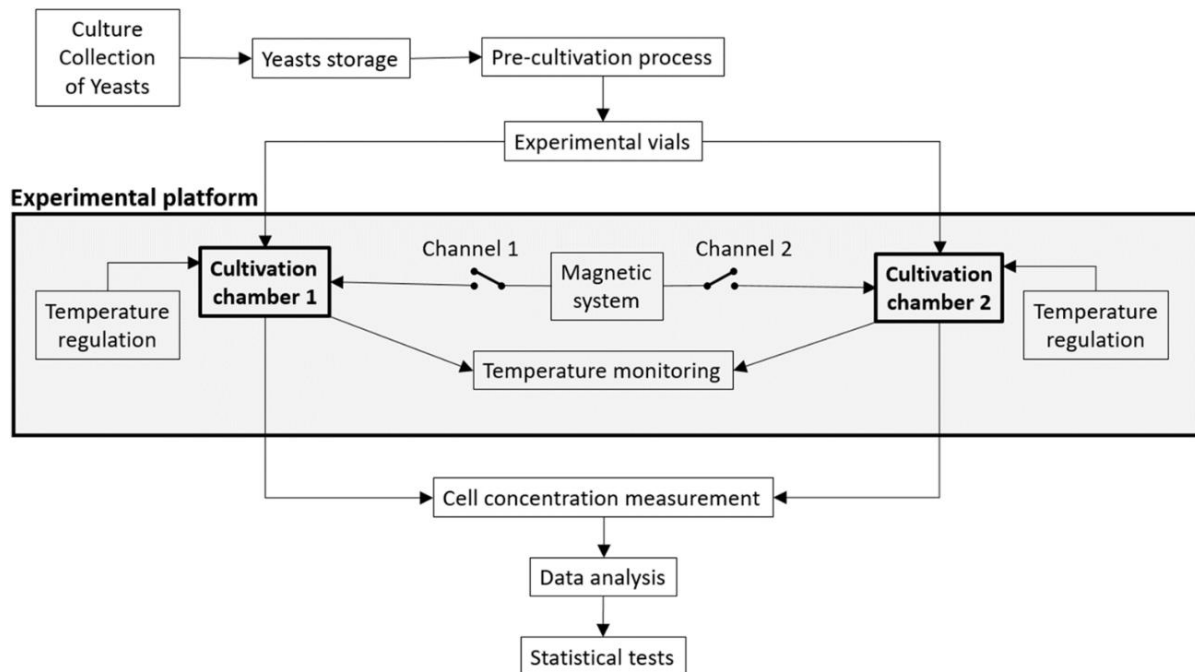


Fig. 1. The workflow diagram illustrates the experimental design, with the experimental platform serving as the central component.

Yeast cell cultivation

- To determine the optimal starting cell concentration, vials containing 11.7 ml of pre-culture were serially diluted in 10-fold increments with YPD medium and incubated for 20 hours. For more refined dilution experiments, the final volume in each vial was increased to 13 ml, and the incubation time was shortened to 18 hours. To maintain constant temperature conditions, all experiments in the two thermal chambers involved vials immersed in a water bath.
- To study the overall growth curve of the yeast cells under controlled chamber conditions, a diluted yeast pre-culture in YPD medium was divided into two sets of 42 vials, each containing 13 ml of culture. At each measurement point, three vials per chamber were taken for analysis.
- To evaluate cell growth under experimental conditions, the pre-culture was diluted in YPD medium and divided into 10 vials, each containing 13 ml of culture. Two sets of 5 vials each were placed in separate cultivation chambers, within Helmholtz coils. Yeast cells were cultivated with or without exposure to MF, depending on the experimental conditions.

3. RESULTS

In this section, we describe the developed experimental platform in detail, focusing on both the hardware and the biological features that are crucial for its proper functioning. The platform consists of four key components: a pair of custom-adjusted cultivation chambers, a precise temperature regulation system, a MF generation unit, and a central control and data acquisition unit. In addition, an optical microscope (Kern OCL-2, Kern & Sohn, Germany) fitted with a digital

camera (FLC 1600H, Do3thing, China) was used to count the cells and check the microbiological purity of the samples. In the following sections, outline the main features of these components and the optimal conditions for yeast cell growth are described to ensure a comprehensive understanding of the system's overall design and capabilities.

Magnetic system

The magnetic system Fig. 2 for generating MF consists of two independent channels, each of which is responsible for supplying MF to one of the cultivation chambers. At its core is a signal generator (Owon, XDG3102, China), which is equipped with two channels, each of which generates alternating current signals. These signals are directed to a dedicated amplifier (NX3000D, Behringer, Germany), which has two separate inputs and outputs that allow independent amplification for each channel.

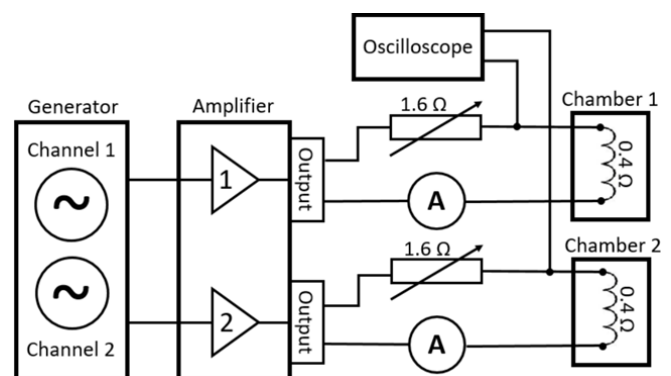


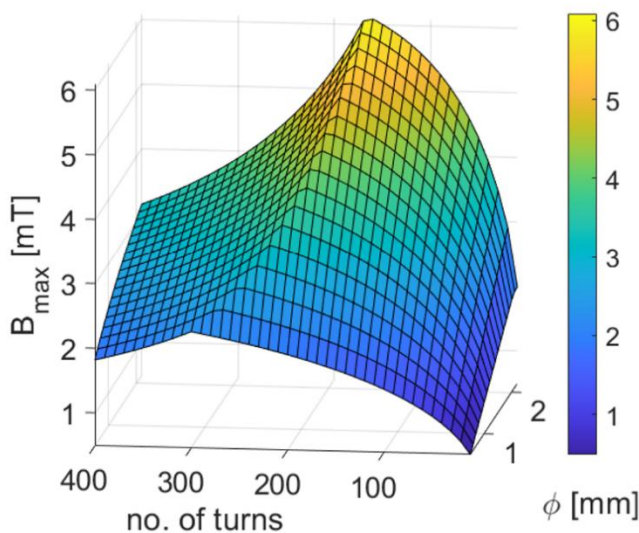
Fig. 2. Schematic diagram of the MF generation system, illustrating the signal generator, amplifier, rheostats, Helmholtz coils in two chambers, and an oscilloscope with ammeters.

After amplification, the signals are routed through a rheostat, which – together with the 0.4Ω resistance of the Helmholtz coils – can be set to a total resistance of 2Ω , ensuring that the system impedance conforms to the amplifier. An oscilloscope (Owon, XDS3102, China) is connected to both channels, allowing real-time visualization of the waveforms and verification of frequency and amplitude. An ammeter is connected in series in each circuit to monitor the electrical current. This configuration ensures stable control of the MF throughout the exposure period. In addition, the MF system offers flexibility as MF activation can occur in either one or both chambers simultaneously, depending on the experimental requirements.

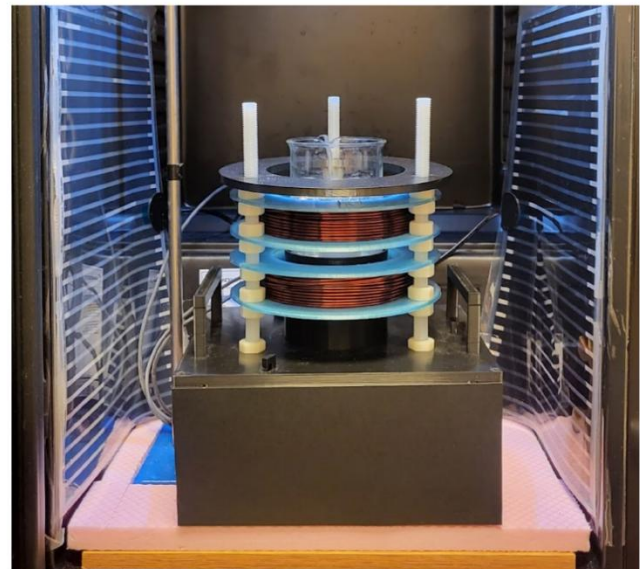
A quasi-homogeneous MF from Helmholtz coils was developed for the cell culture exposure. The coil parameters (coil diameter, wire diameter, number of turns, and number of wire layers) were optimized within the specified MF frequency range (Hz-kHz) and heat production of the coils ($\leq 2 \text{ W}$) by modeling in MATLAB (version R2023b, MathWorks, Inc.) (Fig. 3(a)), with the aim of maximizing magnetic flux density in the center of the coils. Since the

impedance and power dissipation increase with more turns, the amplifier cannot keep the current constant. We also had to enforce a strict power dissipation limit to prevent the chamber from overheating, resulting in the non-monotonic field curve shown in (Fig. 3(a)). The modeling led to the construction of two coils with a 110 mm diameter, made of 2.2 mm copper wire with 50 turns each (Fig. 3(b)). The inductance of the coils was 0.4 mH at 1 kHz. The coil support and other accessories were 3D printed.

The arbitrary waveform generator provides an adjustable frequency and amplitude for the MF. The signal amplifier enhances AC currents up to 8 A (rms) to generate MF in the frequency range of 0-2 kHz, achieving a magnetic flux density of up to 5 mT. In the central part of the coils, where the biological experiment takes place, the homogeneity of MF is 95 %, as experimentally verified with a gaussmeter (model 5180, F.W. BELL, USA) at 15 equidistant points covering the entire experimental volume. Identical coils were placed in both chambers to ensure the same conditions. The measured maximum difference between the MFs was up to 1 %.



(a)



(b)

Fig. 3. (a) Modeling of the maximum magnetic flux density as a function of the number of coil turns and the wire diameter. (b) Details of the Helmholtz coils and the foil heating system on the chamber walls.

Temperature regulation

The customized thermal chambers were developed using a glass-door refrigerator (Candy CCV 150 EU, Italy). The housing consists of a steel sheet outer shell, polyurethane (PUR) foam insulation, and an inner ABS plastic lining. The dimensions of the appliance are 500 mm (width) \times 560 mm (depth) \times 840 mm (height), with an effective internal volume of 122 l. The chambers were heated with heating foils (Ultratherm Viv Mat 22, UK) attached to both side walls of the chamber (Fig. 3(b) and Fig. 4(a)). The measured contribution of the foils to the MF inside the coils was below the detection limit (0.005 mT); therefore, its impact on our experimental setup can be considered negligible. The

temperature was controlled by a PID temperature controller (Rex C100V Pt100, rKc Instrument, Japan) equipped with a sensor that was immersed in the water bath holding the experimental vials. In addition, a temperature monitoring system was implemented using a microcontroller board (Arduino UNO Rev3, Italy) with four digital temperature sensors (DS18B20, Analog Devices, Inc., USA) and a sampling period of 10 s.

A series of temperature distribution tests were carried out inside the chamber, with several sensors placed simultaneously at different locations. Here we show one such test performed with a PID controller set to $35 \text{ }^\circ\text{C}$: one sensor was immersed in the water bath containing vials of water,

while two other sensors were positioned at different heights within the chamber (Fig. 4(a)). Fig. 4(b) shows the inhomogeneous temperature distribution in the chamber. Initially, the system required time to stabilize, reaching different steady-state levels and exhibiting different thermal dynamics over time. Although temperature differences of more than 5 °C were observed between the different parts of the chamber, the submerged sensor in the water bath consistently recorded stable values. The depicted test scenario was more challenging as the coils were active and served as an additional heat source. Nevertheless, the target temperature of 35 °C was successfully maintained, which corresponded to the conditions observed when the coils were inactive. Under these control conditions, the temperature distribution within the chamber exhibited a more typical gradient, with temperatures gradually increasing from the bottom to the top of the box.

The temperature curves clearly show that it is necessary to place the temperature sensor used for regulation directly at

the sample location – a practice that has not been consistently followed in similar studies. The initial overshoot of about 0.6 °C observed in the red curve was the result of the PID controller's response to opening the incubator and placing the preheated samples (almost 35 °C) in a water bath that had already stabilized at 35 °C. This transient temperature rise was unavoidable under the given conditions. More importantly, similar overshoots were recorded simultaneously in both chambers, regardless of whether they were under test or control conditions. As a result, not only was the mean sample temperature of 35 ± 0.3 °C achieved in both chambers, but also the mean temperature difference between the two chambers remained within ± 0.3 °C throughout the experiment.

Based on these tests, the "regulation" and monitoring sensors were placed close to each other and exclusively in the water bath of each cultivation chamber to monitor the temperature of the yeast samples.

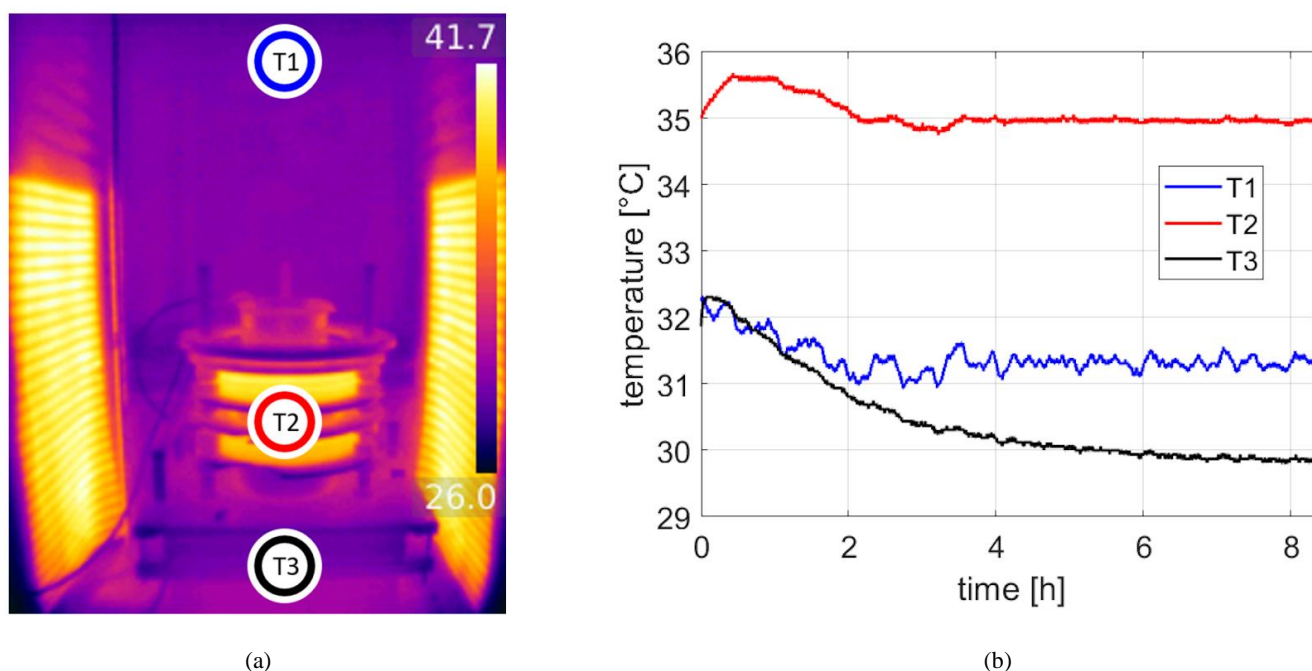


Fig. 4. (a) Thermal image of the cultivation chamber. (b) Temperature stability test in the chamber with the PID controller set to 35 °C. T1 – top of the cultivation chamber, T2 – water bath in the beaker, T3 – bottom of the cultivation chamber.

Optimal starting microbial concentration

For the optimal experimental setup, two interdependent parameters had to be determined: the initial cell concentration and the total cultivation time. As these parameters could not be determined simultaneously, they were determined iteratively. On the one hand, extending the duration of the experiment increases the probability of detecting the MF effect. On the other hand, practical considerations, such as limiting each run to a single day (24 h), result in a maximum cultivation window of approximately 20 hours, allowing at least 2 hours for preparation and post-experiment procedures. Knowing this approximate time frame, the next step was to look for suitable dilution levels that would allow the cells to remain in the desired growth phase during the available cultivation period.

In the search for the optimum initial concentration of *Saccharomyces cerevisiae* CCY 21-4-99, biomass growth was first assessed after 20 hours of stationary cultivation at 35 °C as a function of the initial cell density. The biomass growth, which was measured turbidimetrically (turbidimeter Lutron TU-2016, Taiwan), was expressed as a percentage relative to the 24-hour pre-culture (Fig. 5). The data show that only the sample containing 10 % of the pre-culture (i.e., a 1:10 dilution) achieved a biomass equivalent to 100 % of the pre-culture. In contrast, biomass growth of 50 % or less was observed at dilutions greater than $1:3.2 \times 10^4$, indicating a significant decrease in growth. At a dilution of $1:10^7$, biomass growth was already negligible (2.2 %), illustrating the sensitivity of growth to lower initial cell density.

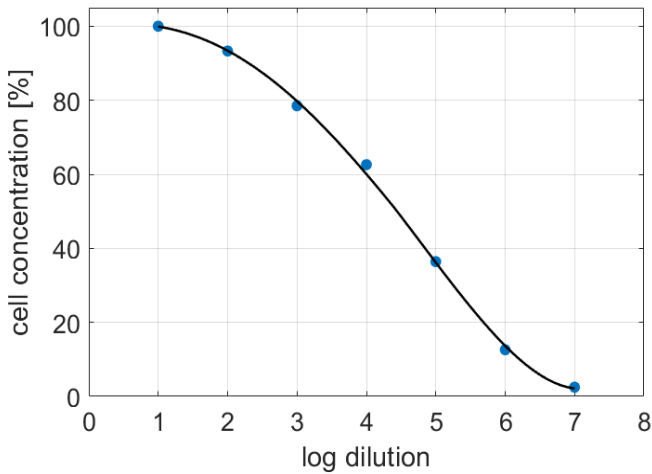


Fig. 5. Cell concentration (●) after 20 hours of cultivation as a function of the initial inoculum dilution.

Our target window for final biomass growth was between 20-60 %, as detecting differences in paired experiments becomes more challenging when final concentrations are either too low or too high (see explanation below and Fig. 6(b)). To further refine this range, we tested pre-culture dilutions from 5×10^4 to 2×10^5 . Based on these experiments, the final pre-culture concentration corresponded to a 1.8×10^5 -fold dilution of the original pre-culture (results not shown), which corresponds to a calculated value of 306 cells/ml.

Modeling the optimal duration of a biological experiment

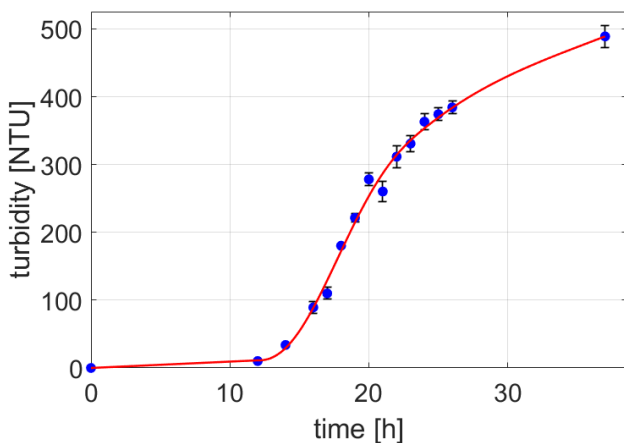
For the selected initial cell concentration (306 cells/ml), the culture was cultivated in parallel in two identical thermostatic chambers, and biomass growth was monitored over time. The yeast cell concentrations were measured turbidimetrically from the 12th hour onwards, with a total of 14 measurement time points. At each time point, samples were taken from three vials per chamber. In this way, two growth curves were simultaneously obtained, one in each

chamber. The data shown represent mean values of these two curves, fitted with a sixth-order polynomial, including an extrapolation to a single point at 36 hours (Fig. 6(a)).

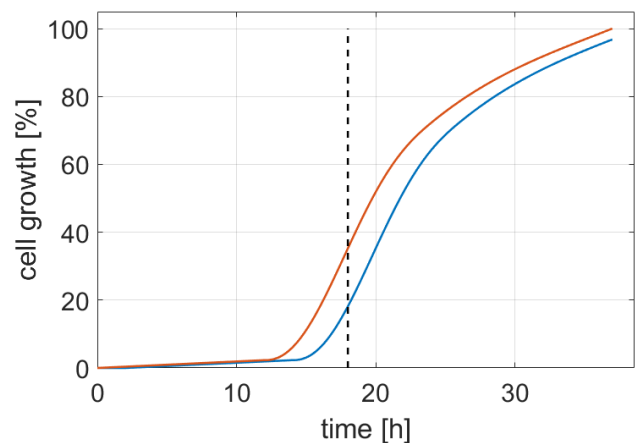
The cell growth curve shows that the biomass levels remained below half of the fully developed biomass at 37 hours until the 19th hour. In particular, the data show that the exponential growth phase continued until the 19th hour, with the biomass levels remaining below 50 % of the stationary phase maximum (Fig. 6(a)). During this early growth period, the biomass doubled within approximately 2 hours or less. Such a growth curve is characteristic of stationary cultivation, where the cells grow at the bottom of the vials without mixing or agitation.

Next, it was necessary to determine a specific time point at which to terminate the experiment – a crucial step in optimizing the experimental design. The goal was to estimate a time range that would maximize the probability of detecting differences between the magnetic field and control conditions. Without this consideration, the most promising time window for observing potential effects could be missed, especially if the effect is subtle. Therefore, we attempted to estimate the optimal time point at which the differences are most pronounced and therefore most likely to be detectable. Otherwise, even if an effect were present, it could remain undetected if the measurements were taken at suboptimal time points.

To guide this decision, we used a simple modeling approach based on the assumption that any environmental influence, including MF, could shift the growth curve over time: either to the left (implying stimulation) or to the right (implying inhibition). The direction of the shift was not critical for this purpose. Rather, the goal was to determine the time point at which the difference between the shifted and unshifted curves is most pronounced. In Fig. 6(b), the blue curve illustrates the inhibition scenario, where the growth process is delayed by 2 hours compared to the original red curve.



(a)



(b)

Fig. 6. (a) Growth curve showing the increase in cell concentration of *Saccharomyces cerevisiae* CCY 21-4-99 at 35 °C over time (error bars \pm SD). (b) Simulation of MF impact by delaying growth by 2 hours (blue curve). The vertical line at 18th h indicates the moment of maximum difference between the two growth curves.

The scenario illustrated clearly shows that for shorter experiment durations ($t < \sim 13$ h), the two curves do not diverge sufficiently to detect differences. Conversely, for longer durations ($t > \sim 25$ h), the curves begin to converge, and the differences become smaller. Thus, the largest gap occurs within an intermediate time window of 15-25 hours. Additional modeling with different time shifts – including minimal shifts on the order of 0.1 h – was performed to simulate subtle differences, as the goal was to develop a platform sensitive enough to capture small MF effects. Ultimately, the experiment duration was set at 18 hours under the given conditions, during which the yeast population underwent an estimated 16 consecutive doublings.

Testing a paired experimental design

In this section, we present the proof of concept for the developed experimental platform. The paired experiment was conducted over a period of 18 hours, with five test sample vials placed in each chamber and operated in two modes: (1) both chambers under control conditions without MF, and (2) both chambers exposed to a 50 Hz MF of 3.5 mT, driven by an electric current of 4.5 A. The temperature in both cultivation chambers was maintained at 35 °C throughout the experiment.

For each experimental run, the environmental conditions were evaluated using three parameters: the mean temperature in chamber 1, the mean temperature in chamber 2, and the mean temperature difference between the two chambers. Only experimental runs that met the following three temperature criteria were included in further analysis: the mean temperature in chamber 1 and in chamber 2 had to remain within 35 ± 0.3 °C and the mean temperature difference between the chambers had to be within ± 0.3 °C.

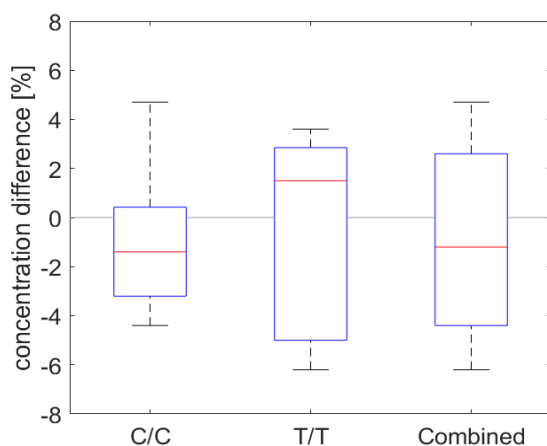


Fig. 7. Boxplots for cell concentration differences between cultivated cultures in two chambers.

C/C: both chambers in control mode without MF ($N = 5$).

T/T: both chambers in test mode with MF ($N = 5$).

Combined: merged data from the two previous sets ($N = 10$).

In Fig. 7, the cell concentration difference between the cultures in the two chambers in a paired experimental setup is illustrated by boxplots for three data sets: simultaneous

operation of both chambers in control mode with MF switched off ($N = 5$), both chambers in test mode with MF switched on ($N = 5$), and a combined set merging the previous two ($N = 10$). In all three cases, the mean difference in cell growth between the two chambers remained below 1 %. Statistical analysis using a one-sample t-test did not reject the hypothesis that the mean values of these sets were equal to zero (p -values = 0.56, 0.78, and 0.52, respectively). These results indicate that the two chambers provide sufficiently consistent conditions for cell growth within the given experimental settings.

4. DISCUSSION

The experimental platform was specifically designed to overcome critical challenges commonly encountered in studies investigating LF MF effects on biological systems. A cornerstone of the platform design is the ability to maintain tightly controlled and reproducible experimental conditions through the integration of standardized or customized components.

Temperature regulation and monitoring are particularly important, as even minor fluctuations can significantly affect biological responses regardless of MF exposure. A deviation of as little as 1 °C can significantly affect biological growth and potentially lead to the effects being misattributed to MF exposure. In contrast to the detailed temperature management protocols presented in this study, most previous research has paid insufficient attention to this critical variable.

To ensure accurate temperature control in the present study, the sensors were directly immersed in the water bath containing the biological samples, allowing for real-time, localized temperature measurement. This configuration also helps to mitigate the thermal gradients generated by active components such as Helmholtz coils and heating elements, which could otherwise affect the environmental uniformity. Careful optimization of the chamber architecture further minimized these thermal disturbances.

Although the authors of numerous studies speak of satisfactory thermal control, they often lack quantitative evidence, such as a statistical characterization of the temperature time series or direct comparisons of measured temperatures between test and control locations. Of the relevant studies that investigated the effects of 50/60 Hz MF on biological systems ([2]-[4], [7], [11], [29]-[31]), only two ([2], [30]) monitored temperature at both test and control sites. Of these studies, only one ([2]) provided quantification, and even this was limited to reporting a temperature range with no mean values or standard deviations. As a result, none of the reviewed studies reported the actual measured temperature differences between the experimental groups. In addition, none of the studies performed internal consistency checks, such as control-control or test-test comparisons, to confirm that the paired setups provided equivalent conditions. Similarly, no crossover design was used in any study to eliminate potential site-specific biases between the paired systems.

The temperature monitoring integrated into our experimental platform also showed exceptional thermal stability throughout the experimental runs. Variations within and between chambers remained minimal, ensuring a consistent and uniform environment for all biological samples. The simultaneous operation of both chambers further confirmed their suitability for high-precision, reproducible paired experiments.

In our study, we used a single-wrapped coil design, which results in an asymmetry in heat generation due to the active coils in the test chamber. However, we ensured thermal symmetry between both chambers through PID temperature regulation, precise temperature monitoring, and the exclusion of experimental runs that did not meet strict temperature uniformity criteria. In principle, a double-wrapped coil configuration could mitigate heating by balancing the current flow, with both the control and test conditions carrying the same current but in opposite directions (anti-parallel in one case, parallel in the other), resulting in equivalent heat generation.

The operation of electromagnetic coils is often associated with mechanical vibrations that can affect sensitive biological experiments. Both coil configurations, single- and double-wrapped, are subject to this vibration phenomenon [32]. In both cases, the vibrations occur when a non-zero resulting MF is present, i.e. during exposure of the test sample. When a double-wrapped coil is fed with antiparallel currents, resulting in a zero magnetic field (which corresponds to our "control" condition), no vibrations are observed [32], similar to our system's control state, where the coils are turned off. This shows that we are not able to create identical vibration conditions for the "magnet on" and "magnet off" states.

In agreement with the above, a faint buzzing noise was observed during coil operation in our setup, indicating the presence of low-level vibrations. However, the microbial culture vials were located in water baths housed in larger beakers, which helped to partially attenuate the mechanical vibrations transmitted by the coils. In addition, the yeast cells used in the experiments consistently settled at the bottom of the vials during incubation, regardless of whether MF was switched on or off. This indicates that the vibrations were not sufficient to resuspend the cells and noticeably improve their access to nutrients and oxygen, factors that could otherwise have a noticeable effect on biomass growth.

The yeast strain *Saccharomyces cerevisiae* CCY 21-4-99 was selected as the model organism for this study due to its unique and advantageous characteristics. This non-pathogenic, thermotolerant strain thrives at an optimal growth temperature of 35 °C, which coincides with the operating temperature range of the experimental platform. Its eukaryotic cell structure provides a relevant model for the study of biological processes similar to those in higher organisms, offering distinct advantages over prokaryotic models such as bacteria.

Mathematical modeling and growth rate analyses were used to determine the optimal duration and initial cell concentration of *Saccharomyces cerevisiae* CCY 21-4-99, ensuring that cells remained in the growth phase during MF

exposure. Keeping the cells in a physiologically active state is critical for two reasons: it increases their responsiveness to MF exposure and minimizes confounding factors such as cellular aging and decreasing viability.

In the final tests, growth differences between the *Saccharomyces cerevisiae* CCY 21-4-99 cultures in the two chambers were minimal and statistically insignificant, demonstrating the technological readiness of the platform for precise and reliable paired experiments. In addition, the platform allows simultaneous exposure of multiple samples in a single run. However, the use of stationary cell cultures is a potential limitation, as these conditions differ from stirred or agitated cultures and potentially affect nutrient distribution and aeration.

Although we used a specific yeast strain in this study, the platform can be similarly applied to various prokaryotic or eukaryotic microorganisms, as well as subcellular components such as enzymes. Furthermore, the whole approach can be technically adapted to different experimental requirements, including modifications to different electromagnetic field sources (such as permanent magnets), temperature regulation, stirring, or cell concentration monitoring.

5. CONCLUSION

We have developed a robust and adaptable experimental platform that overcomes the main methodological challenges in studying LF MF effects on biological systems. By ensuring precise control over environmental variables such as temperature and MF homogeneity, the platform significantly improves experimental reliability and reproducibility and addresses the limitations observed in previous studies. The modular design provides flexibility for diverse experimental requirements, including adaptation to different electromagnetic field sources and biological models.

Future improvements will include real-time monitoring of cell biomass and viability by electrical impedance spectroscopy, further expanding the platform's capabilities. Future investigations will explore a wider range of MF parameters, such as frequency, magnetic flux density, and pulse mode, to deepen our understanding of LF MF interactions at the cellular, subcellular, and biochemical levels. This high-precision experimental system provides a valuable basis for further exploration of MF-induced biological effects and their potential applications in biomedicine and biotechnology.

CONFLICT OF INTERESTS

The authors declare no competing interests.

ACKNOWLEDGMENT

This research was supported by research grant 2/0160/25 from the VEGA Grant Agency. We thank Dr. Renáta Vadkertiová from the Institute of Chemistry of SAS for selecting and kindly providing the appropriate yeast strain from the Culture Collection of Yeasts.

AUTHOR'S CONTRIBUTIONS

H.V.: Conceptualization (equal), Methodology (equal), Investigation (lead), Formal analysis (equal), Software (equal – implementation of data analysis), Data curation (equal), Writing-original draft (equal).

L.K.: Conceptualization (equal), Methodology (equal), Investigation (equal), Formal analysis (equal), Writing-original draft (equal), Resources (equal), Supervision (equal).

M.B.: Conceptualization (equal), Methodology (equal), Writing-original draft (equal).

M.T.: Conceptualization (equal), Methodology (equal), Investigation (equal), Formal analysis (lead), Software (lead – implementation of data analysis), Data curation (equal), Writing-original draft (equal), Funding acquisition, Resources (equal), Supervision (equal).

DATA AVAILABILITY

The data that support the findings of this study are available within the article and upon reasonable request.

REFERENCES

- [1] Tota, M., Jonderko, L., Witek, J., Novickij, V., Kulbacka, J. (2024). Cellular and molecular effects of magnetic fields. *International Journal of Molecular Sciences*, 25 (16), 8973. <https://doi.org/10.3390/ijms25168973>
- [2] Lee, H. C., Hong, M.-N., Jung, S. H., Kim, B. C., Suh, Y. J., Ko, Y.-G., Lee, Y.-S., Lee, B.-Y., Cho, Y.-G., Myung, S.-H., Lee, J.-S. (2015). Effect of extremely low frequency magnetic fields on cell proliferation and gene expression. *Bioelectromagnetics*, 36 (7), 506-516. <https://doi.org/10.1002/bem.21932>
- [3] Zhang, M., Li, X., Bai, L., Uchida, K., Bai, W., Wu, B., Xu, W., Zhu, H., Huang, H. (2013). Effects of low frequency electromagnetic field on proliferation of human epidermal stem cells: An in vitro study. *Bioelectromagnetics*, 34 (1), 74-80. <https://doi.org/10.1002/bem.21747>
- [4] Pasi, F., Sanna, S., Paolini, A., Alquati, M., Lascialfari, A., Corti, M. E., Di Liberto, R., Cialdai, F., Monici, M., Nano, R. (2016). Effects of extremely low-frequency magnetotherapy on proliferation of human dermal fibroblasts. *Electromagnetic Biology and Medicine*, 35 (4), 343-352. <https://doi.org/10.3109/15368378.2016.1138123>
- [5] Radil, R., Carnecka, L., Judakova, Z., Pobocikova, I., Bajtos, M., Janousek, L. (2024). Exploring non-thermal mechanisms of biological reactions to extremely low-frequency magnetic field exposure. *Applied Sciences*, 14 (20), 9409. <https://doi.org/10.3390/app14209409>
- [6] Lai, H. (2021). Genetic effects of non-ionizing electromagnetic fields. *Electromagnetic Biology and Medicine*, 40 (2), 264-273. <https://doi.org/10.1080/15368378.2021.1881866>
- [7] Duong, C. N., Kim, J. Y. (2016). Exposure to electromagnetic field attenuates oxygen-glucose deprivation-induced microglial cell death by reducing intracellular Ca²⁺ and ROS. *International Journal of Radiation Biology*, 92 (4), 195-201. <https://doi.org/10.3109/09553002.2016.1136851>
- [8] Caliozna, L., Medetti, M., Bina, V., Brancato, A. M., Castelli, A., Jannelli, E., Ivone, A., Gastaldi, G., Annunziata, S., Mosconi, M., Pasta, G. (2021). Pulsed electromagnetic fields in bone healing: Molecular pathways and clinical applications. *International Journal of Molecular Sciences*, 22 (14), 7403. <https://doi.org/10.3390/ijms22147403>
- [9] Gualdi, G., Costantini, E., Reale, M., Amerio, P. (2021). Wound repair and extremely low frequency-electromagnetic field: Insight from in vitro study and potential clinical application. *International Journal of Molecular Sciences*, 22 (9), 5037. <https://doi.org/10.3390/ijms22095037>
- [10] Sun, J., Tong, Y., Jia, Y., Jia, X., Wang, H., Chen, Y., Wu, J. Jin, W., Ma, Z., Cao, K., Li, X., Chen, Z., Yang, G. (2023). Effects of extremely low frequency electromagnetic fields on the tumor cell inhibition and the possible mechanism. *Scientific Reports*, 13 (1), 6989. <https://doi.org/10.1038/s41598-023-34144-5>
- [11] Xu, A., Wang, Q., Lin, T. (2020). Low-frequency magnetic fields (LF-MFs) inhibit proliferation by triggering apoptosis and altering cell cycle distribution in breast cancer cells. *International Journal of Molecular Sciences*, 21 (8), 2952. <https://doi.org/10.3390/ijms21082952>
- [12] Wang, S., Zhou, X., Huang, B., Wang, Z., Zhou, L., Wang, M., Yu, L., Jiang, H. (2016). Noninvasive low-frequency electromagnetic stimulation of the left stellate ganglion reduces myocardial infarction-induced ventricular arrhythmia. *Scientific Reports*, 6 (1), 30783. <https://doi.org/10.1038/srep30783>
- [13] Rick, O., von Hehn, U., Mikus, E., Dertinger, H., Geiger, G. (2017). Magnetic field therapy in patients with cytostatics-induced polyneuropathy: A prospective randomized placebo-controlled phase-III study. *Bioelectromagnetics*, 38 (2), 85-94. <https://doi.org/10.1002/bem.22005>
- [14] Brabant, C., Geerinck, A., Beaudart, C., Tirelli, E., Geuzaine, C., Bruyere, O. (2023). Exposure to magnetic fields and childhood leukemia: A systematic review and meta-analysis of case-control and cohort studies. *Reviews on Environmental Health*, 38 (2), 229-253. <https://doi.org/10.1515/reveh-2021-0112>
- [15] Baaken, D., Dechent, D., Blettner, M., Drießen, S., Merzenich, H. (2021). Occupational exposure to extremely low-frequency magnetic fields and risk of amyotrophic lateral sclerosis: Results of a feasibility study for a pooled analysis of original data. *Bioelectromagnetics*, 42 (4), 271-283. <https://doi.org/10.1002/bem.22335>
- [16] Dasdag, O., Adalier, N., Dasdag, S. (2020). Electromagnetic radiation and Alzheimer's disease. *Biotechnology & Biotechnological Equipment*, 34 (1), 1087-1094. <https://doi.org/10.1080/13102818.2020.1820378>
- [17] Tian, H., Zhu, H., Gao, C., Shi, M., Yang, D., Jin, M., Wang, F., Sui, X. (2023). System-level biological effects of extremely low-frequency electromagnetic fields: An in vivo experimental review. *Frontiers in Neuroscience*, 17, 1247021. <https://doi.org/10.3389/fnins.2023.1247021>

- [18] Sincak, M., Luptakova, A., Matusikova, I., Jandacka, P., Sedlakova-Kadukova, J. (2023). Application of a magnetic field to enhance the environmental sustainability and efficiency of microbial and plant biotechnological processes. *Sustainability*, 15 (19), 14459. <https://doi.org/10.3390/su151914459>
- [19] Liu, J., Wang, D., Wang, H., Yang, N., Hou, J., Lv, X., Gong, L. (2024). Low frequency magnetic field assisted production of acidic protease by *Aspergillus niger*. *Archives of Microbiology*, 206, 273. <https://doi.org/10.1007/s00203-024-04004-5>
- [20] Bodewein, L., Schmiedchen, K., Dechent, D., Stunder, D., Graefrath, D., Winter, L., Kraus, T., Driessen, S. (2019). Systematic review on the biological effects of electric, magnetic and electromagnetic fields in the intermediate frequency range (300 Hz to 1 MHz). *Environmental Research*, 171, 247-259. <https://doi.org/10.1016/j.envres.2019.01.015>
- [21] Buchachenko, A. (2016). Why magnetic and electromagnetic effects in biology are irreproducible and contradictory? *Bioelectromagnetics*, 37 (1), 1-13. <https://doi.org/10.1002/bem.21947>
- [22] International Commission on Non-Ionizing Radiation Protection (ICNIRP). (2025). Gaps in knowledge relevant to the “ICNIRP guidelines for limiting exposure to time-varying electric, magnetic and electromagnetic fields (100 kHz TO 300 GHz)”. *Health Physics*, 182 (2), 190-202. <https://doi.org/10.1097/HP.0000000000001944>
- [23] Makinistian, L., Vives, L. (2025). Devices, facilities, and shielding for biological experiments with static and extremely low frequency magnetic fields. *IEEE Journal of Electromagnetics, RF and Microwaves in Medicine and Biology*, 9 (2), 141-156. <https://doi.org/10.1109/JERM.2024.3419232>
- [24] Ronniger, M., Aguida, B., Stacke, C., Chen, Y., Ehnert, S., Erdmann, N., Eschenburg, G., Falldorf, K., Pooam, M., Wing, A., Ahmad, M. (2022). A novel method to achieve precision and reproducibility in exposure parameters for low-frequency pulsed magnetic fields in human cell cultures. *Bioengineering*, 9 (10), 595. <https://doi.org/10.3390/bioengineering9100595>
- [25] Bereta, M., Teplan, M., Chafai, D. E., Radil, R., Cifra, M. (2021). Biological autoluminescence as a noninvasive monitoring tool for chemical and physical modulation of oxidation in yeast cell culture. *Scientific Reports*, 11, 328. <https://doi.org/10.1038/s41598-020-79668-2>
- [26] Vu Viet, H., Teplan, M. (2023). Development of an experimental platform for the measurement of biological response of low-frequency magnetic fields. In *2023 14th International Conference on Measurement*. IEEE, 113-116. <https://doi.org/10.23919/MEASUREMENT59122.2023.10164326>
- [27] Bajla, I., Teplan, M. (2022). Yeast cell detection in color microscopic images using ROC-optimized decoloring and segmentation. *IET Image Processing*, 16 (2), 606-621. <https://doi.org/10.1049/ipr2.12376>
- [28] Bereta, M., Teplan, M., Zakar, T., Vuviet, H., Cifra, M., Chafai, D. E. (2024). Biological autoluminescence enables effective monitoring of yeast cell electroporation. *Biotechnology Journal*, 19 (4), 2300475. <https://doi.org/10.1002/biot.202300475>
- [29] Novák J., Strašák, L., Fojt, L., Slaninová, I., Vetterl, V. (2007). Effects of low-frequency magnetic fields on the viability of yeast *Saccharomyces cerevisiae*. *Bioelectrochemistry*, 70 (1), 115-121. <https://doi.org/10.1016/j.bioelechem.2006.03.029>
- [30] An G.-Z., Xu, H., Zhou, Y., Du, L., Miao, X., Jiang, D.-P., Li, K.-C., Guo, G.-Z., Zhang, C., Ding, G.-R. (2015). Effects of long-term 50Hz power-line frequency electromagnetic field on cell behavior in Balb/c 3T3 cells. *PLoS One*, 10 (2), e0117672. <https://doi.org/10.1371/journal.pone.0117672>
- [31] Song K., Im, S. H., Yoon, Y. J., Kim, H. M., Lee, H. J., Park, G. S. (2018). A 60 Hz uniform electromagnetic field promotes human cell proliferation by decreasing intracellular reactive oxygen species levels. *PLoS One*, 13 (7), e0199753. <https://doi.org/10.1371/journal.pone.0199753>
- [32] Jones, R. A., Walleczek, J., Adey, W. R. (1996). Mechanical vibration in “double-wound” magnetic field exposure coils. *Bioelectromagnetics*, 17 (6), 516-518. [https://doi.org/10.1002/\(SICI\)1521-186X\(1996\)17:6%3C516::AID-BEM14%3E3.0.CO;2-I](https://doi.org/10.1002/(SICI)1521-186X(1996)17:6%3C516::AID-BEM14%3E3.0.CO;2-I)

Received February 18, 2025

Accepted May 6, 2025